Biomedical Signal Processing and Control 80 (2023) 104263

Contents lists available at ScienceDirect

Biomedical Signal Processing and Control

journal homepage: www.elsevier.com/locate/bspc

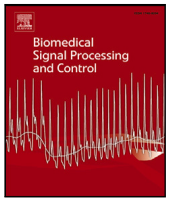

Comparison of classification techniques for the control of EOG-based HCIs

Alberto López [a,*], José R. Villar [b], Marta Fernández [a], Francisco J. Ferrero [a]

[a] Department of Electrical and Electronic Engineering, University of Oviedo, Spain
[b] Department of Computer Science, University of Oviedo, Spain

ARTICLE INFO

Keywords:
Classification
Ensemble of classifiers
Electrooculogram
Human–computer interface
Machine learning

ABSTRACT

Electrooculogram (EOG) is the measurement of the biopotential generated by eye movement. These signals are crucial for people with severe motor disabilities because they rarely suffer alterations in eye movement. Therefore, the correct classification of these signals could find application in the design of simple user interfaces that allow independence and communication skills. This paper presents a comparison of the main classification techniques in the literature for the control of EOG-based human–computer interfaces (HCIs). Static threshold, K-nearest neighbor (KNN), artificial neural network (ANN), and support vector machine (SVM) techniques, together with two new ensembles of classifiers. One is based on a voting scheme while the other employs two stages to encode the outcomes from the KNN, SVM, and ANN classifiers. All classifiers were compared based on four parameters – precision, specificity, sensitivity, and accuracy – to select the most appropriate approach in real-time. This work also provides a novel data set consisting of signals from nine healthy participants and compares the above methods also on another public data set. Machine learning-based models proved to be more robust for continuous use of an EOG-based HCI, while static thresholds are better for specific and repetitive actions.

1. Introduction

The Electrooculogram (EOG) is a measurement of the electrical activity of the ocular globule. In 1848 the German physicist Emil du Bois-Reymond observed that the eye behaved like a dipole, where the cornea could be modeled as the positive pole and the retina as the negative pole, so that eye movement gave rise to variations in the potential of said dipole [1]. This record of ocular activity is used as a diagnostic tool for pathologies in the oculomotor system [2] such as sleep disturbances [3], neurodegenerative diseases [4], or in the equilibrium sense test known as the Hallpike caloric test [5]. In addition, it can be a reliable source of commands, since, through proper treatment, it is possible to achieve a unique relationship between the direction of the gaze and an action to be performed. In this sense, several systems have been developed in which the control is carried out according to the direction of the gaze. Based on this idea, systems have been developed that favor personal autonomy [6], such as control of robot arms [7], prostheses [8], and electric wheelchairs [9].

Fig. 1 shows a typical EOG signal by recording the potential difference between the eyes in two separate channels: horizontal and vertical. Saccadic eye movements can be distinguished with a typical amplitude of 7 μV for each degree of rotation of the eyeball. As the greatest angle of rotation is around 100°, signals up to approximately 700 μV of amplitude can be identified according to du Bois Reymond studies [10]. The EOG bandwidth is between continuous and 50 Hz [11]. The straight-ahead look is shown as a flat signal, while the up/right looks are shown as positive potential and the down/left as negative potential. These identified patterns within the signal constitute the motif to classify. Note that eye blinks can also be labeled; these eye blinks are those that are consciously performed and not those caused by reflex movements. However, when the eye is centered, both channels are within the vicinity of a certain threshold. This threshold varies from one user to another or even for the same user according to his/her current activity, level of stress, or tiredness [12].

An EOG-based system includes at least four stages: signal acquisition, a preprocessing stage that comprises signal denoising and feature extraction, signal classification, and decision-making or application. The signal is acquired by surface electrodes and once the EOG signal has been denoised it is processed to extract and classify the information it contains. Last, a decision is made based on the classification and the target application.

The most significant works in the field of EOG signal classification are presented in Table 1. On the one hand, there are those that have addressed the problem themselves by proposing classical machine learning (ML) methods: K-Nearest Neighbor (KNN), Support Vector Machines (SVM), Artificial Neural Networks (ANN), and Decision Trees (DT) without being oriented to any application. On the other

* Corresponding author.
E-mail address: uo181549@uniovi.es (A. López).

https://doi.org/10.1016/j.bspc.2022.104263
Received 16 April 2022; Received in revised form 30 August 2022; Accepted 19 September 2022
Available online 13 October 2022

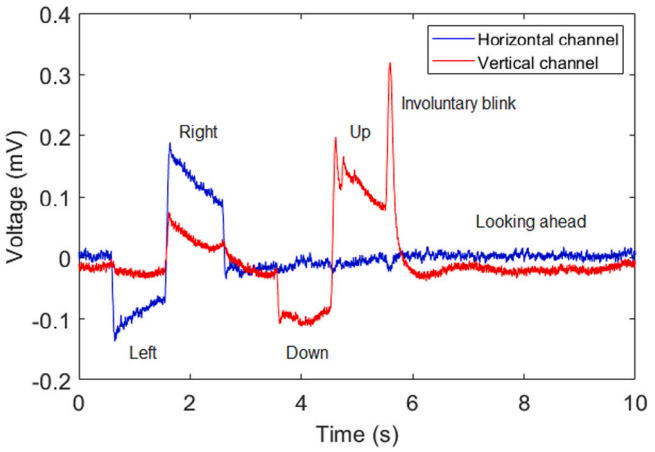

Fig. 1. Typical EOG labeled with the corresponding position the eyes are focusing on.

Table 1
Most significant works in the field of EOG signal classification by employing thresholds and classical ML methods.

Authors	Methods	Accuracy (%)
Güven and Kara [16]	ANN	94.1
Bulling et al. [17]	SVM	76.1
Mala et al. [18]	SVM	83.3
Dong et al. [19]	SVM	96.1
Qi et al. [20]	ANN, SVM	69.8
Rakshit et al. [21]	KNN, SVM, Ensemble	90.0
O'Bard and George [22]	KNN, SVM, DT	96.9
Park et al. [23]	Static threshold	94.0
Aungsakun et al. [24]	Static threshold	100
Wu et al. [25]	Dynamic threshold	88.6
Soltani et al. [26]	Dynamic threshold	93.0
Saravanakumar et al. [27]	Dynamic threshold	98.0

hand, there are those that have addressed it from the perspective of controlling human-computer interfaces (HCIs) using thresholds as the classification method. As the EOG signals are slightly different for each subject, dynamic threshold algorithms have started to be considered in recent works. The corneal–retinal dipole potential also depends on the illumination of the environment in which the recording is made. The amplitude of the potential increases in the dark while it decreases in bright light [13–15]. In both cases, good performance has been obtained without offering a thought comparative study like the one carried out in this work for the control of EOG-based HCIs.

In this research, the analysis of EOG systems in two different scenarios are analyzed in the experimentation: on the one hand, the short-term actions, where repetitive simple tasks are performed; on the other hand, the long-term actions as a sequence of simple movements one after the other. Furthermore, a two-stages classifier that includes an ensemble of well-known methods and the posterior classification is proposed. This method is compared with state-of-the-art published solutions. The differences in the performance of the methods for the two scenarios provide an idea of how the research would lead to improving this type of sensory system. Some main findings of this research are that it tests and provides insights into the performance of different classification approaches, including ensemble voting methods for the most common EOG device usage patterns: short-term repetitive and long-term complex. This research also found that there is no such winning classification method when considering mixed usage patterns, typical in the everyday use of EOG devices.

This study is structured as follows. Next section deals with the description of the EOG two-stages classifier. Section 3 includes the experimental setup, data sets, and cross-validation scheme. Afterwards, Section 4 copes with the results and the discussion on them. The study ends by concluding this research.

2. An ensemble for EOG signal classification

EOG classification is defined as the task of classifying the EOG signal of each channel into one of the possible classes. Considering L_H labels for the horizontal channel and L_V labels for the vertical one, the domain can be divided into $L_H \times L_V$ mutually exclusive areas. For this study, each channel is analyzed independently.

Experimenting with the different published proposals for EOG signal classification leads to wonder how the long-term evaluations can be faced using the available alternatives. As shown later in the experimentation, long-term evaluations of the models show worse performance than when considering short-term ones. This research proposes a new classifier that considers classical ML methods as label suggestions for the current signal under evaluation; in a second stage, all these inputs are labeled using a KNN classifier, alleviating the problem of worsening the performance with the length of the experiment. Fig. 2 shows the block diagram of the proposal.

As mentioned before, the idea is to create an ensemble of classifiers that assist the final classification stage in the decision-making process. Instead of using a classical voting scheme for the ensemble, the classifier outcomes are considered as new inputs for the second stage. The first classification stage includes three different classifiers trained for the same task: assigning a label to each EOG channel input. The difference between the three classifiers meets the ensemble's requirement so the aggregation does not introduce bias.

The three selected ML models for the first classification stage are KNN, SVM, and feed-forward Neural Network. The main reason for choosing these ML models is that they have been reported in the literature to successfully cope with the EOG channel signal labeling. Also, these models can be easily deployed on embedded devices provided the models are carefully trained and pruned when necessary. This might be important for the KNN model, where selecting the most representative samples severely reduces the retained training instances, thus, reducing both the needed storage and the processing time.

KNN is an algorithm that searches the closest observations to the one it is trying to predict and classifies the point of interest based on most of the surrounding data. In this case, the number of neighbors is the main parameter to set. SVM constructs a set of hyper-planes dividing the domain space to keep the instances from each class in totally separated spaces. In this implementation the problem is subdivided into M sub-problems, with M the number of labels, in a one-versus-one coding; the coefficients for mixing the one-to-one models are obtained using an optimization algorithm as explained in [28].

Finally, ANN is an interconnected group of nodes, inspired by a simplification of neurons in the brain. Each node receives input from other nodes or an external data source. Each input has an associated weight that is modified in the learning process. Each node applies a function of the sum of the inputs weighted by the weights. The only parameter set here is the number of nodes to consider in the neural network trying different values and looking for the one that returns the best performance.

The outcomes from these three classifiers are codified using one-hot-encoder. That is, the outcome from classifier i at stage 1 is o_{1i} $\forall i \in \{1, \ldots, C\}$ with the probability of labeling the instance with class i. As long as we have C classes, the outcome is transformed into C variables C_{1j} -$\forall j \in \{1, \ldots, C\}$-, where C_{1j} is o_{1i}.

The second stage includes a single classifier that assigns the final labels to the incoming instances. For this case, a KNN classifier has been chosen because its simplicity; however, any other classifier would be valid provided the available data is large enough for its training. The inputs to this classifier are: (i) the EOG channel signal, (ii) the C outcomes from each of the first stage classifiers.

The classifying ensemble scheme is replicated -and trained- for each EOG channel. Only three classes are considered in each channel: DOWN, CENTER, or UP for the vertical channel, and LEFT, CENTER, or RIGHT for the horizontal one. For the training and testing of this proposal, we assume that each instance (a filtered EOG signal sample) is labeled with one of these classes. All the signal pre-processing is done before the classification stage.

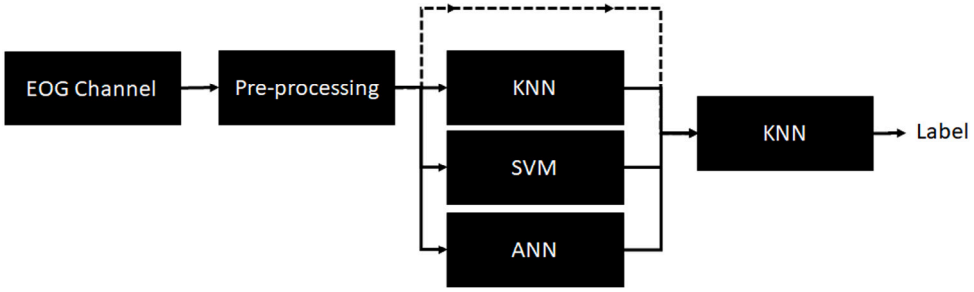

Fig. 2. Block diagram of the ensemble proposed in this research. The EOG signal is pre-processed and labeled with three different ML models. Their outcomes, together with the pre-processed variables, represent the inputs to the second stage classifier. This last model assigns the final label to the signal.

3. Experimental set up

This section deals with the description of the experiments to evaluate the performance of the ensemble from the previous section, hereafter referred as *EOG2SC*, acronym of EOG two stages classifier. First, the description of the data sets used in this study and their main characteristics are detailed. Afterwards, the battery of methods to compare our solution with will be described. Finally, the performance measurements will be explained.

3.1. Experimental set up and data

In this work, two data sets for the evaluation of the proposals are proposed: one focused on long-term actions and a second one including short-term actions.

- **Long-term actions data set**: the UNIOVI-EOG data set. This data set is completely defined in Appendix A. The UNIOVI-EOG data set has been specially designed and gathered for this experimentation in our laboratory at the University of Oviedo using the BlueGain EOG device [29]. This bioamplifier provides a test software application for signal display, filtering, digitization, and wireless transmission to the computer. The signals of nine healthy participants (seven males and two females) with a mean age of 28.3±5.4 years were recorded using this device and following the well-defined protocol exposed in Appendix A.1. This study was approved by the department's ethics board, and all participants signed the consent form in advance.
  The EOG signals go through high-pass and low-pass filters −30 Hz and 0.1 Hz, respectively- to eliminate noise from the power line and unnoticed reflexive blink artifacts. Next, a smoothing of the signal is performed using a sliding window of size $10/F$, where F is the sampling frequency to reduce the fluctuation of the signal. The pre-processing also includes the data scaling to unify all the measurements of the subjects' behavior. To do so, a calibration stage is needed at the beginning of the use of the device to determine the mean, median, and standard deviation of the eye in a normal position (supposedly when the eye is centered). The output of the pre-processing is expressed by an instance of two variables (H_i, V_i), filtered and scaled within the interval [–0.8; 0.8] mV.
  A time series (TS) is composed of eye-tracking sequences for which the horizontal and vertical potential difference is recorded. For each participant, data from one of the ten TS they generated are used to train the models, while the rest TS are used to test them.
- **Short-term actions data set**: the UMALTA-EOG data set, including extremely short and repetitive tasks. This public data set comprises EOG data recorded from six healthy subjects (two males and four females; mean age 24.7±3.1 years) with normal vision. A total of 300 trials were recorded for each subject in three separate sessions with 100 trials recorded in each session. It is necessary to compensate for the drift present in these signals. A high pass filter with a cutoff frequency of 0.001 Hz has been applied to avoid signal distortions instead of the 0.3–0.4 Hz recommended by the paper [30]. Pre-processing also includes the data scaling in the interval [–0.8; 0.8] mV to unify all the measurements.

3.2. Comparison set up

The two completely different above-described scenarios serve to evaluate the performance of the EOG2SC. However, to include a complete comparison, three independent classifiers will be used as well for labeling the EOG channel instances. The selected models are the KNN, the SVM, and the ANN obtained from the training of the EOG2SC. As already mentioned, these classifiers represent state-of-the-art methods in the EOG literature, so analyzing how well these methods perform and comparing them with the EOG2SC would allow extracting conclusions.

As exposed in Table 1, the method that reports the best performance in the literature is based on a static threshold. This method establishes a static threshold of 50 μV for both channels, reporting accuracy of 100% [24]. This threshold-based method is included in this comparison as long as this is one of the most used methods in the literature; this method is referred to as THRD. Finally, a simple voting ensemble scheme is also considered. In this case, the majority class from the three classifiers is assumed as the final class. In case of a draw, a CENTER class is proposed. From now on, we will refer to this ensemble as VOTING.

Leave-one-participant-out cross-validation scheme is proposed for this comparison. In this scheme, the TS from one participant is kept for validation, while the TS from the remaining participants is used for training the models. Repeating for each different participant we obtain a measurement of the robustness and generalization capabilities of the different solutions compared.

3.3. Performance measurements

The well-known measurements of accuracy, precision, sensitivity, and specificity are used to evaluate the performance of the different modeling techniques; these measurements are calculated using Eqs. (1) to (4), correspondingly. In these equations:

- TP_L (True Positive) counts the instances correctly classified with label L.
- TN_L (True Negative), counts the instances correctly classified as $\neg L$.
- FP_L (False Positive) counts the instances wrongly classified as L.
- FN_L (False Negative) counts the instances wrongly classified as $\neg L$.

$$Accuracy_L = \frac{TP_L + TN_L}{TP_L + FN_L + TN_L + FP_L} \quad (1)$$

$$Precision_L = \frac{TP_L}{TP_L + FP_L} \quad (2)$$

Table 2
UMALTA-EOG data set test results, including the precision, specificity, sensitivity, and accuracy for all the methods. The static threshold is set to 50 μV. The geometric mean of the measurements from both channels is also included as an overall performance metric.

Model	Precision	Specificity	Sensitivity	Accuracy
	Horizontal			
KNN	85.8536	90.0532	78.0370	76.4520
ANN	85.8531	90.0529	78.0355	76.4508
SVM	85.8169	90.0148	77.9296	76.3443
VOTING	85.8520	90.0516	78.0322	76.4474
EOG2SC	85.8534	90.0530	78.0362	76.4512
THRD	**88.2000**	**91.2900**	**82.5900**	**88.2100**
Model	Precision	Specificity	Sensitivity	Accuracy
	Vertical			
KNN	88.0930	**90.4997**	**81.5305**	78.9381
ANN	88.0926	90.4992	81.5249	78.9369
SVM	88.0703	90.4776	81.4755	78.8743
VOTING	88.0918	90.4985	81.5233	78.9348
EOG2SC	88.0930	**90.4997**	**81.5305**	78.9381
THRD	**88.3000**	88.2900	80.3600	**86.5600**
Model	Precision	Specificity	Sensitivity	Accuracy
	Geometric mean			
KNN	86.9661	90.2762	79.7646	77.6851
ANN	86.9656	90.2758	79.7611	77.6839
SVM	86.9363	90.2460	79.6829	77.5990
VOTING	86.9647	90.2748	79.7587	77.6811
EOG2SC	86.9660	90.2760	79.7642	77.6847
THRD	**88.2500**	**90.2900**	**81.4700**	**87.3900**

Table 3
UNIOVI-EOG data set test results, including the precision, specificity, sensitivity, and accuracy for all the methods. The static threshold is set to 50 μV. The geometric mean of the measurements from both channels is also included as an overall performance metric.

Model	Precision	Specificity	Sensitivity	Accuracy
	Horizontal			
KNN	**99.9991**	**99.9996**	**99.9990**	**99.9992**
ANN	99.9863	99.9934	99.9868	99.9875
SVM	99.9216	99.9620	99.9083	99.9192
VOTING	99.9937	99.9968	99.9928	99.9937
EOG2SC	99.9970	99.9985	99.9972	99.9972
THRD	89.6500	90.5600	81.1100	88.4100
Model	Precision	Specificity	Sensitivity	Accuracy
	Vertical			
KNN	**99.9990**	**99.9995**	**99.9991**	**99.9991**
ANN	99.9830	99.9913	99.9817	99.9834
SVM	99.9242	99.9605	99.9137	99.9209
VOTING	99.9911	99.9950	99.9892	99.9903
EOG2SC	99.9948	99.9973	99.9949	99.9949
THRD	88.3000	89.2900	80.3600	86.5600
Model	Precision	Specificity	Sensitivity	Accuracy
	Geometric mean			
KNN	**99.9991**	**99.9995**	**99.9991**	**99.9992**
ANN	99.9847	99.9923	99.9843	99.9854
SVM	99.9229	99.9612	99.9110	99.9201
VOTING	99.9924	99.9959	99.9910	99.9920
EOG2SC	99.9959	99.9979	99.9960	99.9961
THRD	88.9750	89.9250	80.7350	87.4850

$$Sensitivity_L = \frac{TP_L}{TP_L + FN_L} \tag{3}$$

$$Specificity_L = \frac{TN_L}{TN_L + FP_L} \tag{4}$$

Finally, cross-validation was also employed to obtain the best parameter subset for each of the models; as a result, the value of K was set to 3 and 5 nodes were used for the ANN. The SVM parameters were adjusted using the corresponding library in Matlab.

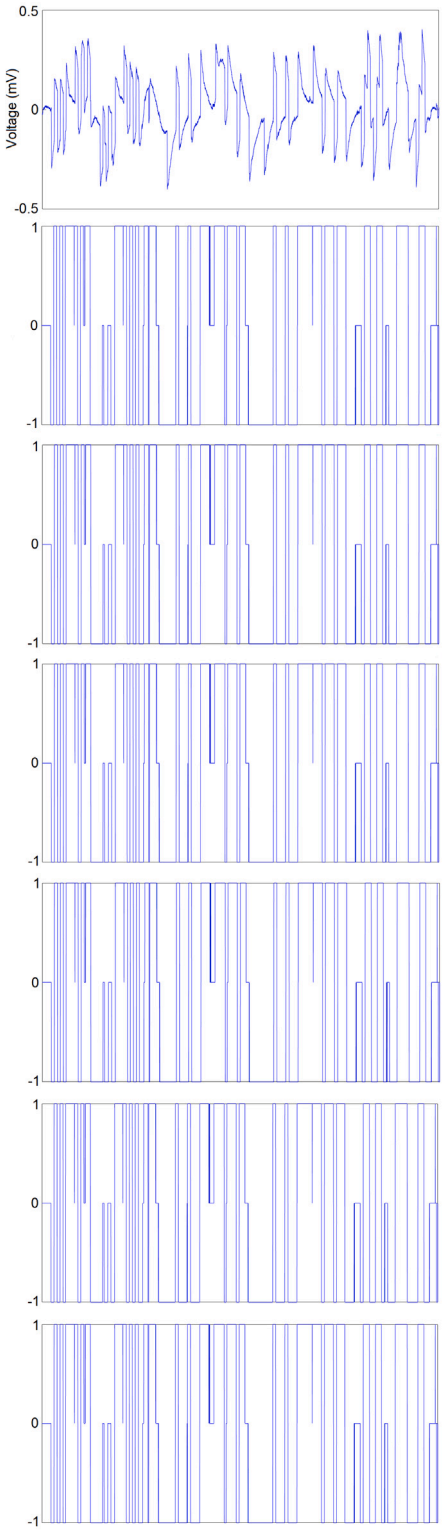

Fig. 3. Original signal, expected classification, and classification using KNN, ANN, SVM, VOTING, and EOG2SC algorithms for the best obtained performance of the horizontal channel. The models were trained with the TS_1^2 and the time period is 130 s.

4. Results and discussion

Results from the experimentation are shown in Tables 2 and 3 for the short-term and long-term sequences of eye movements,

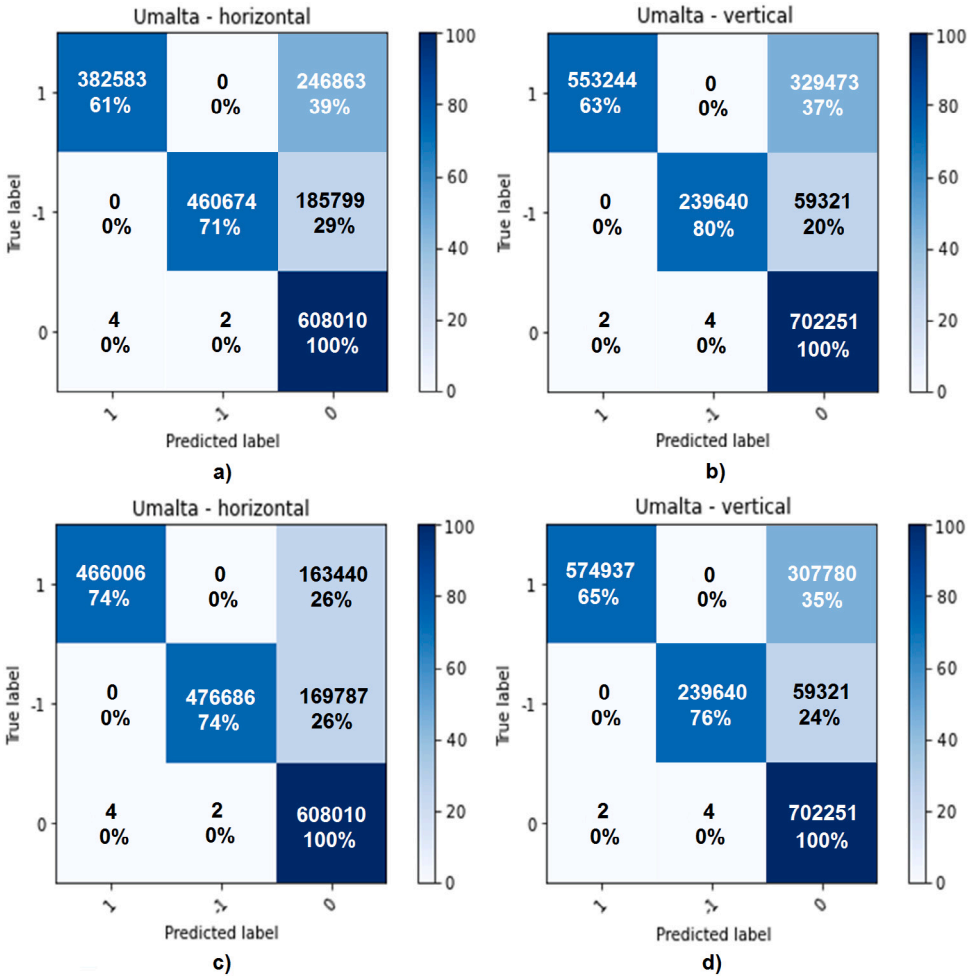

Fig. 4. Confusion matrices using the KNN model [(a) and (b)] and static threshold of 50 μV [(c) and (d)] in horizontal and vertical channels for the UMALTA-EOG data set.

respectively. Table 2 shows the performance obtained by the six methods using the UMALTA-EOG data set. As can be seen, all methods present very similar and consistent results. The threshold-based method has better performance than the ML-based methods in this scenario because simple and repetitive tasks are performed in this data set, always starting from the center of the screen, with small resting periods. This implies that the peaky signal is obtained, free of noise and without fatigue signs; in this case, a threshold seems to be enough for classifying the eye movement. Table 3 shows the performance of the methods when trained and evaluated with the UNIOVI-EOG data set. Because this data set is focused on long-term eye activity, the threshold-based method fails in labeling the signals successfully. On the other hand, the results obtained with the ML-based method are very similar; it cannot be concluded which one method is better than the others given that the difference between them is of the order of 10^{-5}. Due to these small differences, the choice of the best method will be based on the available computational resources. These ML methods offer better performance values than those reported in the literature. Fig. 3 shows the evolution of the horizontal channel for the best classification of the UNIOVI-EOG data set. The actual label and the classification made by the models are also depicted.

Conversely, the UNIOVI-EOG dataset is oriented to continuous tasks without a clear pattern, being much more complicated to follow. Because of this, the threshold-based method performs worse than the ML-based ones. An average value for precision, specificity, sensitivity, and accuracy of 88.56%, 90.11%, 81.10%, and 87.44%, respectively, was obtained employing the static threshold in both data sets. The UMALTA-EOG is more representative in terms of specific actions on interfaces, but for continued use, it is the UNIOVI-EOG. A person using an EOG-based system generally does not have rest times but is constantly viewing and generating eye movements.

Figs. 4 and 5 show the confusion matrices using the KNN model and the static threshold in horizontal and vertical channels for the two data sets considered. Besides, Fig. 6 shows the box plot of the performance of the ML methods for the UMALTA-EOG data set. Considering this, the results show that:

1. There are important differences in the performance of the EOG classification methods according to whether repetitive or prolonged movements with or without resting periods are carried out by the participant.
    - The UMALTA-EOG is a data set oriented to extremely short and repetitive tasks, this data set is more representative of actions on small interfaces.
    - Conversely, the UNIOVI-EOG data set is oriented to continuous and prolonged tasks, without a clear pattern, being much more complicated to follow. This data set might better reflect tasks whose number of steps is bigger and or does not accept resting in the center of the interface.
2. Changes produced in the value of the signals in long-term activities suggest that using thresholds would eventually lead to worse results than when using any of ML methods.

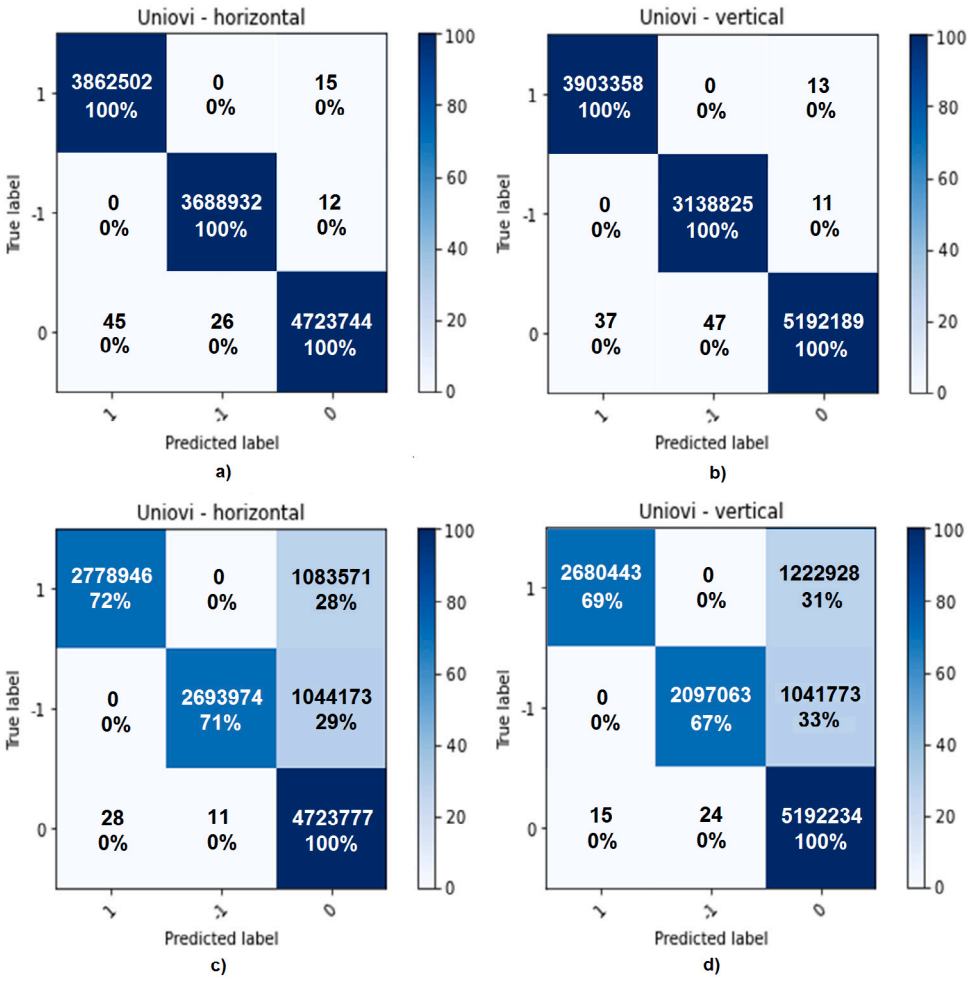

Fig. 5. Confusion matrices using the KNN model [(a) and (b)] and static threshold of 50 μV [(c) and (d)] in horizontal and vertical channels for the UNIOVI-EOG data set.

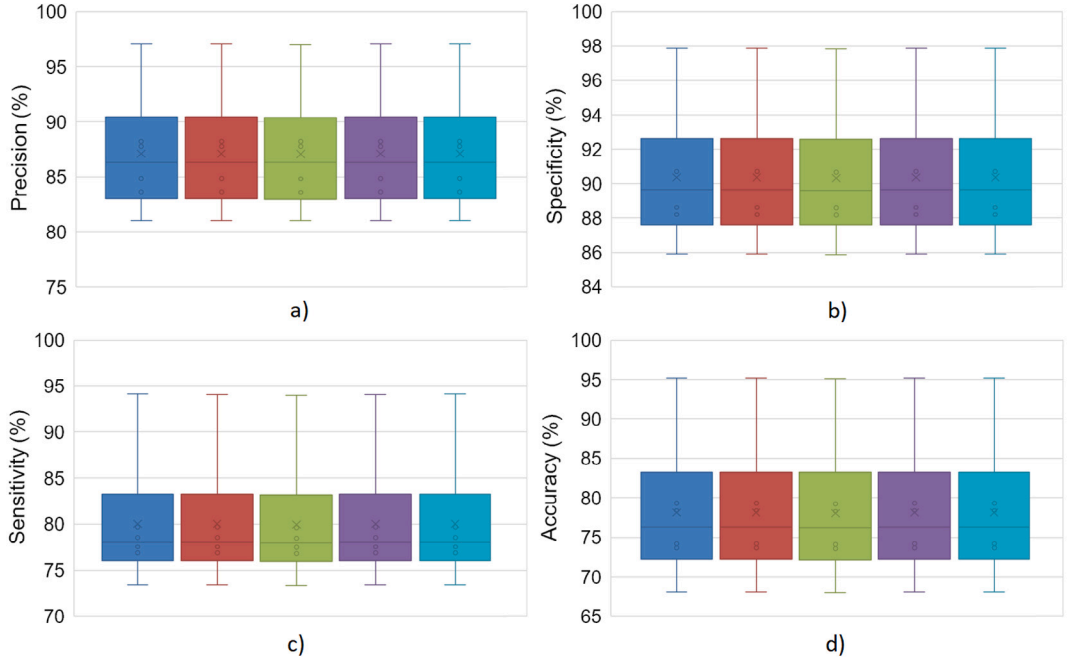

Fig. 6. Box plot of the (a) precision, (b) specificity, (c) sensitivity, and (d) accuracy of results for the six subjects of the UMALTA-EOG data set. On each graph and from left to right: KNN, ANN, SVM, VOTING, and EOG2SC.

3. For short-term activity the best method in terms of average is the threshold, but all the methods are statically similar. For long-term activity, the threshold-based method is statically worse than the ML methods.

It is important to remark that some of the current uses of EOG interfaces are related to closed-eyes EOG, such as security access control [31]. However, open-eyes EOG still has a lot of applications, such as in robotic control [32], cognitive overload detection [33] or even in driving safety [34]. Recent research has been published suggesting that EOG still has a promising use in the industry.

Concerning the benefits of the ensemble proposal, in our opinion, it is not the direct application of this method that can be the future research line. Lessons that this paper suggests include, firstly, that there is a major agreement between the different ML methods when it comes to assessing an instance with a label; otherwise, the ensemble would possibly perform better than any of the individual ML methods. This is an interesting outcome that leads to the second suggested lesson. Provided the results for the KNN with the UNIOVI-EOG dataset (KNN is almost perfect), research must focus on the short-term actions reflected in the UMALTA-EOG, with a rather poor performance for all the methods. In the case of short-term actions, Hidden Markov models can cope with the changes in the state better than any other ML method.

Besides the mentioned issues, future work includes if it is possible to discriminate which type of activities the participant is performing then it could be possible to dynamically select the best model to use. Concerning the models, it seems that Recurrent Networks and Hidden Markov models could be a valid model candidate to cope with the changes due to fatigue in the signals. However, it is important to gather data sets with a higher number of participants and include a variety of activities, so the changes from high-intensity eye activity sequences to repetitive task sequences can be studied as well. Longer TS could also be interesting to enhance the models for coping with less restricted movements. Another challenge is to integrate these classifiers into other applications developed in our research group [35]. The ultimate goal is to provide these EOG-based applications with a better user experience, making them easier and faster to use.

5. Conclusions

This work presents the study carried out to compare the main classification techniques in the literature for the control of EOG-based human–computer interfaces. Static threshold, K-Nearest Neighbor, Artificial Neural Network, and Support Vector Machines techniques, together with two ensembles (one based on a voting scheme and the other based on a two stages classifier). They were compared based on precision, sensitivity, specificity, and accuracy parameters.

From the results obtained using two independent data sets, three main aspects must be considered to select the most suitable technique: (1) the types and variety of eye activities that the EOG-based system must classify and the computational capabilities of the computerized unit. (2) The more complex ML models would produce better performance with the complexity of the movements to identify. (3) Recurrent Neural Networks and Hidden Markov models would eventually produce good results but only based on having enough representative data for the training stages.

CRediT authorship contribution statement

Alberto López: Conceptualization, Writing – original draft, Investigation, Software. **José R. Villar:** Conceptualization, Writing – original draft, Methodology, Funding. **Marta Fernández:** Software, Visualization, Data curation, Investigation. **Francisco J. Ferrero:** Supervision, Preparation, Validation, Writing – review & editing.

Declaration of competing interest

The authors declare that they have no known competing financial interests or personal relationships that could have appeared to influence the work reported in this paper.

Data availability

I have shared my data at the Attach File step.

Acknowledgments

This research has been funded by the Spanish Ministerio de Economía e Industria de España, grant PID2020-112726RB-I00, by the Agencia Estatal de Investigación (AEI, Spain) under grant agreement RED2018-102312-T (IA-Biomed), and by the Ministerio de Ciencia e Innovación CERVERA Excellence Network project CER-20211003 (IBERUS). Also, by Principado de Asturias, grant SV-PA-21-AYUD/2021/50994.

Appendix A. The UNIOVI-EOG data set

EOG classification is defined as the task of classifying the signal in one of the nine possible positions shown in Fig. A.7a. The aim is to find the decision boundaries that define the labels. These boundaries are ideally depicted in Fig. A.7a following a similar design to the one defined for the interfaces shown in Fig. A.8. Variations in the signals due to tiredness or stress would penalize the classification performance; however, these disturbances are not considered.

Two channels (the horizontal -H- and the vertical -V- channels shown in Fig. A.7b) were considered to measure the evolution of the EOG employing the most common electrode placement. These channels represent the difference of potential in each direction. Each channel is labeled with three labels: LEFT, CENTER and RIGHT for the horizontal channel, DOWN, CENTER and UP for the vertical channel.

The protocol followed (see Appendix A.1) includes (1) a resting period, (2) the first series of eye movements tracking a square on a screen, (3) a resting period, (4) a second set of eye movements following a square on a screen, and (5) a final resting period. It is worth mentioning that the two series of eye movements are different and that they were developed in an animated Microsoft PowerPoint file designed by us. Fig. A.9 shows the setup for signal recording. The volunteers sat 60 cm away from the screen on which the activities to be carried out are projected; a 22" LG screen (model 22MT47D; 507×316 mm) was used. The computer screen is positioned parallel to the volunteer's face and at a 90° angle to the table during data recording.

The horizontal and vertical channels were simultaneously sampled at 1 KHz sampling frequency. Each record of the EOG signal following the protocol lasts approximately 4.5 min, while the intermediate resting period lasts 23 s. A time series (TS) is recorded for each of the five repetitions of the experiment. An example of these TS is shown in Fig. A.10, where the upper and the bottom part depict the first and second series of eye movements, respectively, during a run. The TS was automatically segmented with human supervision. Each participant made five recordings; each one was anonymously stored and labeled. The labeled TS was manually split in two TS by the resting period, which was discarded. This separation is performed based on the start and end signals of each TS. Therefore, the data set includes 10 TS for each participant, p; we denote $\{TS_i^p\}\ \forall i \in \{0, 9\}$.

A.1. The sequence of actions

Let us assume $T_1 = 1$ s, $T_2 = 0.5$ s and, $T_3 = 3$ s.

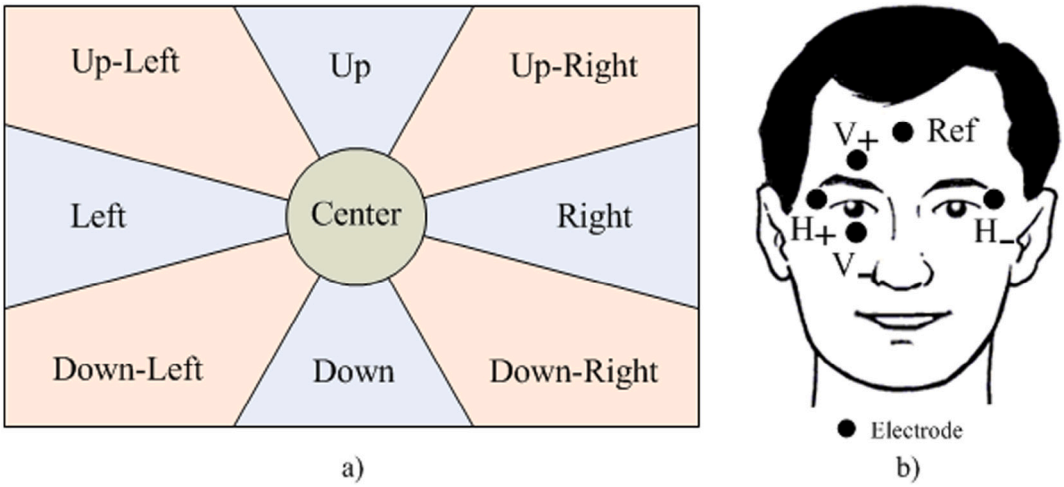

Fig. A.7. (a) Labels defined for the classification issue and decision boundaries; (b) Placement of electrodes to measure the EOG in two separate channels, horizontal -H- and vertical -V-.

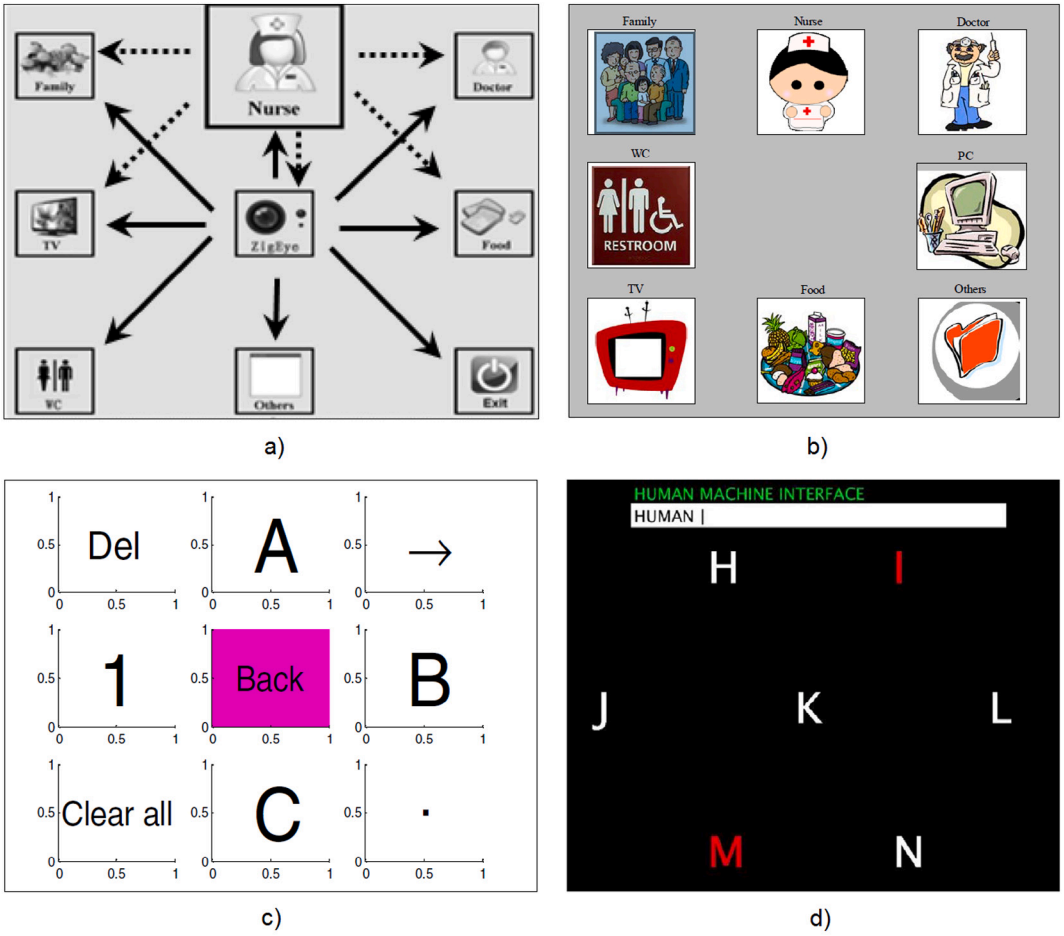

Fig. A.8. Some of the most significant HCIs proposed in the literature in which the interface has been divided into several regions associated with command, selectable by gaze (a) [36]; (b) [37]; (c) [26]; (d) [27].

Labels: L_1 lower left corner, L_2 middle left horizontal, L_3 upper left corner, L_4 vertical upper center, L_5 upper right corner, L_6 middle horizontal right, L_7 lower right corner, L_8 vertical lower center, CENTER or L_9 the center position, and BLINK for when a voluntary blink is performed.

Each time series is composed of the following sequences to eye track and for which the horizontal and vertical potential difference is recorded:

- Visit each quick tag. Starting from the center, after a T_1, go to a possible end, wait for a T_1, and return to the center. The possible

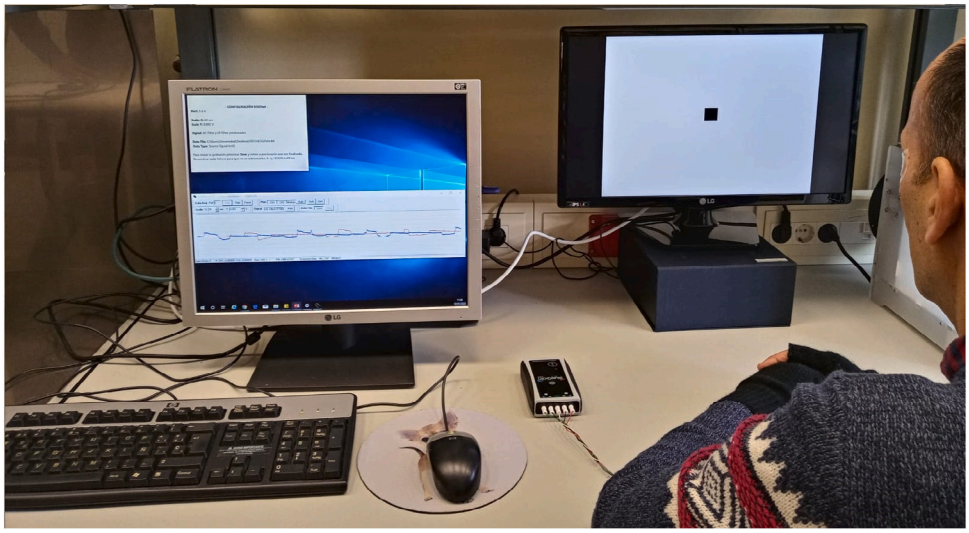

Fig. A.9. EOG signal registry from a volunteer sitting 60 cm away from the screen on which the activities to be carried out are projected.

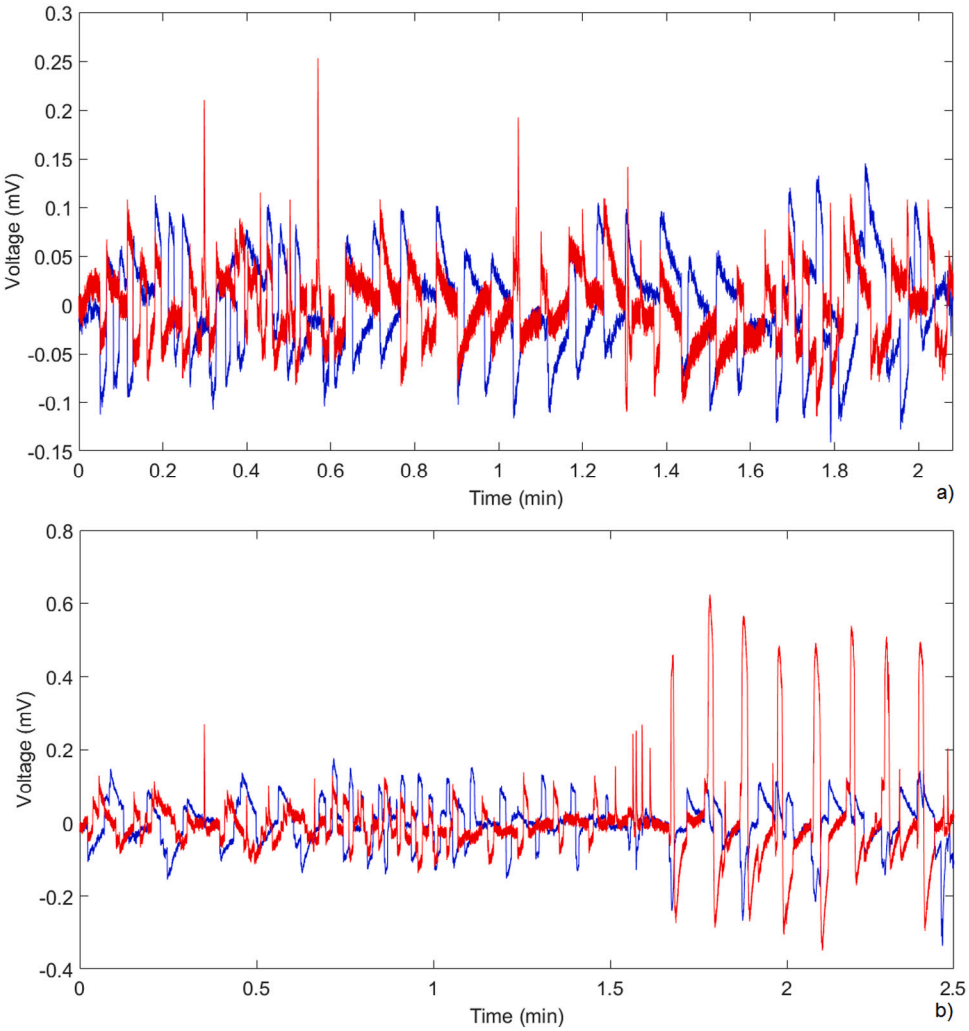

Fig. A.10. Example of the TS performed by each participant. (a) First part of the TS and (b) second part of the TS after the break.

ends are each of the positions shown in Fig. A.7a. There will be two repetitions of this procedure.

- Visit each slow tag. Starting from the center, after a T_1, go to a possible end, wait for a T_3, and return to the center. The possible

ends are each of the positions shown in Fig. A.7a. There will be two repetitions of this procedure.

- Influence of other past actions. Starting from the center, after a T_1, go to a possible end, wait for a T_1, and return to the center. The possible ends are each of the positions shown in Fig. A.7a. The process will be repeated but alternating the destinations following the pattern of L_x-CENTER-L_{x-1}- CENTER-L_x- CENTER-L_{x-1}-CENTER-L_x- CENTER-$L_{(x+4+1)mod8}$ -CENTER and pass through all the labels from L_1 to L_8 (without going through the center).
- Rest for 23 s.
- Travel the perimeter. Starting from the center, after a T_1, go to the different labels, remaining T_1 in each. Sequence: CENTER-$L_1 - L_2 - L_3 - L_4 - L_5 - L_6 - L_7 - L_8$-CENTER-$L_8 - L_7 - L_6 - L_5 - L_4 - L_3 - L_2 - L_1$-CENTER. Repeat twice.
- Main diagonals. Start from the center, and after T_1, go to one corner and from one corner to another. T_1 remains in each. Assuming L_1, L_3, L_5, and L_7 are the corner labels, we will proceed with the following sequence: CENTER-$L_1 - L_5$-CENTER-$L_3 - L_7$-CENTER-$L_5 - L_1$-CENTER-$L_7 - L_3$-CENTER. It will be repeated two times.
- Main horizontals and verticals. Starts from the center, and after T_1, go to the middle left horizontal (L_2) and from this to the opposite end. The central vertical will also proceed. T1 remains in each. Assuming L_2 and L_6 are the left and right horizontal labels and L_4 and L_8 are the vertical labels above and below, we will proceed with the following sequence: CENTER-$L_2 - L_6$-CENTER-$L_4 - L_8$-CENTER-$L_6 - L_2$-CENTER-L_8- L_4-CENTER. It will be repeated two times.
- Visit each quick tag plus blink. Starting from the center, after a T_3, go to a possible end, wait for a T_3, blink, and return to the center and blink. The possible ends are each of the positions shown in Fig. A.7a. There will be two repetitions of this procedure.

Appendix B. Supplementary data

Supplementary material related to this article can be found online at https://doi.org/10.1016/j.bspc.2022.104263.

References

[1] J. Malmivuo, R. Plonsey, Bioelectromagnetism: Principles and applications of bioelectric and biomagnetic fields, 2012, pp. 1–506, http://dx.doi.org/10.1093/acprof:oso/9780195058239.001.0001.

[2] C. Stevenson, T.P. Jung, G. Cauwenberghs, Estimating direction and depth of visual fixation using electrooculography, in: Proceedings of the Annual International Conference of the IEEE Engineering in Medicine and Biology Society, EMBS, Vol. 2015-Novem, 2015, pp. 841–844, http://dx.doi.org/10.1109/EMBC.2015.7318493.

[3] R. Knapp, H. Lusted, Biological signal processing in virtual reality applications, in: Proc. Virtual Reality and Persons with Disabilities, 1993.

[4] R. García-Bermúdez, L.V. Pérez, C. Torres, F.R. Ruiz, J.G. Peñalver, O.V. Cansino, R. Becerra-García, Evaluation of electro-oculography data for ataxia SCA-2 classification: A blind source separation approach, in: Proceedings of the 2010 10th International Conference on Intelligent Systems Design and Applications, ISDA'10, 2010, pp. 237–241, http://dx.doi.org/10.1109/ISDA.2010.5687258.

[5] C.S. Hallpike, The caloric tests, J. Laryngol. Otol. 70 (1) (1956) 15–28, http://dx.doi.org/10.1017/S0022215100052610.

[6] A.B. Usakli, S. Gurkan, Design of a novel efficient human-computer interface: An electrooculagram based virtual keyboard, IEEE Trans. Instrum. Meas. 59 (8) (2010) 2099–2108, http://dx.doi.org/10.1109/TIM.2009.2030923.

[7] A. Úbeda, E. Iañez, J.M. Azorín, An integrated electrooculography and desktop input bimodal interface to support robotic arm control, IEEE Trans. Hum.-Mach. Syst. 43 (3) (2013) 338–342, http://dx.doi.org/10.1109/TSMCC.2013.2241758.

[8] M. Duvinage, T. Castermans, T. Dutoit, Control of a lower limb active prosthesis with eye movement sequences, in: IEEE SSCI 2011 - Symposium Series on Computational Intelligence - CCMB 2011: 2011 IEEE Symposium on Computational Intelligence, Cognitive Algorithms, Mind, and Brain, 2011, pp. 136–142, http://dx.doi.org/10.1109/CCMB.2011.5952116.

[9] A. Banerjee, S. Datta, P. Das, A. Konar, D.N. Tibarewala, R. Janarthanan, Electrooculogram based online control signal generation for wheelchair, in: Proceedings - 2012 International Symposium on Electronic System Design, ISED 2012, 2012, pp. 251–255, http://dx.doi.org/10.1109/ISED.2012.12.

[10] E. Mendelsohn, Physical models and physiological concepts: Explanation in nineteenth-century biology, Br. J. Hist. Sci. 2 (1965) 201–219, http://dx.doi.org/10.1017/S000708740000220X.

[11] J.D. Enderle, Eye movements, in: A. Cohen (Ed.), Encyclopedia of Biomedical Engineering, Wiley, New York, USA, 2006.

[12] J.R. Davis, B. Shackel, Changes in the electro-oculogram potential level, Br. J. Ophthalmol. 44 (1960) 606–618, http://dx.doi.org/10.1136/bjo.44.10.606.

[13] A. Gonshor, R. Malcolm, Effect of changes in illumination level on electro-oculography (EOG), Aerosp. Med. 2 (42) (1971) 138–140, http://dx.doi.org/10.1007/BF00417289.

[14] R. Täumer, N. Rohde, D. Pernice, U. Kohler, EOG: Light test and dark test, Albrecht Von Graefes Arch. Klin. Ophthalmol. 199 (1976) 207–213, http://dx.doi.org/10.1007/BF00417289.

[15] R.P. Borda, Clinical electro-oculography: Optimum illumination levels for the light-adaptation phase, Doc. Ophthal. Proc. Ser. 15 (1978) 147–148, http://dx.doi.org/10.1007/978-94-009-9957-2_24.

[16] A. Güven, S. Kara, Classification of electro-oculogram signals using artificial neural network, Expert Syst. Appl. 31 (1) (2006) 199–205, http://dx.doi.org/10.1016/j.eswa.2005.09.017.

[17] A. Bulling, J.A. Ward, H. Gellersen, G. Tröster, Eye movement analysis for activity recognition using electrooculography, IEEE Trans. Pattern Anal. Mach. Intell. 33 (4) (2011) 741–753, http://dx.doi.org/10.1109/TPAMI.2010.86.

[18] S. Mala, K. Latha, Feature selection in classification of eye movements using electrooculography for activity recognition, Comput. Math. Methods Med. 2014 (2014) http://dx.doi.org/10.1155/2014/713818.

[19] E. Dong, C. Li, C. Chen, An EOG signals recognition method based on improved threshold dual tree complex wavelet transform, in: 2016 IEEE International Conference on Mechatronics and Automation, IEEE ICMA 2016, 2016, pp. 954–959, http://dx.doi.org/10.1109/ICMA.2016.7558691.

[20] L.J. Qi, N. Alias, Comparison of ANN and SVM for classification of eye movements in EOG signals, J. Phys. Conf. Ser. 971 (1) (2018) http://dx.doi.org/10.1088/1742-6596/971/1/012012.

[21] A. Rakshit, A. Banerjee, D.N. Tibarewala, Electro-oculogram based digit recognition to design assitive communication system for speech disabled patients, in: International Conference on Microelectronics, Computing and Communication, MicroCom 2016, 2016, pp. 3–7, http://dx.doi.org/10.1109/MicroCom.2016.7522560.

[22] B. O'Bard, K. George, Classification of eye gestures using machine learning for use in embedded switch controller, in: I2MTC 2018 - 2018 IEEE International Instrumentation and Measurement Technology Conference: Discovering New Horizons in Instrumentation and Measurement, Proceedings, IEEE, 2018, pp. 1–6, http://dx.doi.org/10.1109/I2MTC.2018.8409769.

[23] S. Park, D. Kim, H. Kim, Development of a human-computer interface device using electrooculogram for the amyotrophic lateral sclerosis patient, in: Proceedings of the 3rd European Medical and Biological Engineering Conference, Vol. 11, 2005, pp. 1727–1983, (1).

[24] S. Aungsakun, A. Phinyomark, P. Phukpattaranont, C. Limsakul, Development of robust electrooculography (EOG)-based human-computer interface controlled by eight-directional eye movements, Int. J. Phys. Sci. 7 (14) (2012) 2196–2208, http://dx.doi.org/10.5897/ijps11.1486.

[25] S.L. Wu, L.D. Liao, S.W. Lu, W.L. Jiang, S.A. Chen, C.T. Lin, Controlling a human-computer interface system with a novel classification method that uses electrooculography signals, IEEE Trans. Biomed. Eng. 60 (8) (2013) 2133–2141, http://dx.doi.org/10.1109/TBME.2013.2248154.

[26] S. Soltani, A. Mahnam, Design of a novel wearable human computer interface based on electrooculograghy, in: 2013 21st Iranian Conference on Electrical Engineering, ICEE 2013, 2013, http://dx.doi.org/10.1109/IranianCEE.2013.6599876.

[27] D. Saravanakumar, M.R. Reddy, A high performance asynchronous EOG speller system, Biomed. Signal Process. Control 59 (2020) 101898, http://dx.doi.org/10.1016/j.bspc.2020.101898.

[28] MathWorks, Fit multiclass models for support vector machines or other classifiers, 2022, https://es.mathworks.com/help/stats/fitcecoc.html, accessed: 2022-05-24.

[29] B.C.R. Systems, BlueGain EOG biosignal amplifier, 2021, [Web; accessed 01-06-2021]. URL http://www.crsltd.com/tools-for-vision-science/eye-tracking/bluegain-eog-biosignal-amplifier/.

[30] N. Barbara, T.A. Camilleri, K.P. Camilleri, A comparison of EOG baseline drift mitigation techniques, Biomed. Signal Process. Control 57 (2020) 101738, http://dx.doi.org/10.1016/j.bspc.2019.101738.

[31] R.D. Findling, T. Quddus, S. Sigg, Hide my gaze with eog! 2019, pp. 107–116, http://dx.doi.org/10.1145/3365921.3365922.

[32] K. Sharma, N. Jain, P.K. Pal, Detection of eye closing/opening from EOG and its application in robotic arm control, Biocybern. Biomed. Eng. 40 (1) (2020) 173–186, http://dx.doi.org/10.1016/j.bbe.2019.10.004.

[33] J. Morton, A. Zheleva, B.B. Van Acker, W. Durnez, P. Vanneste, C. Larmuseau, J. De Bruyne, A. Raes, F. Cornillie, J. Saldien, L. De Marez, K. Bombeke, Danger, high voltage! Using EEG and EOG measurements for cognitive overload detection in a simulated industrial context, Applied Ergon. 102 (2022) 103763, http://dx.doi.org/10.1016/j.apergo.2022.103763.

[34] Y. Jiao, F. Jiang, Detecting slow eye movements with bimodal-LSTM for recognizing drivers' sleep onset period, Biomed. Signal Process. Control 75 (2022) 103608, http://dx.doi.org/10.1016/j.bspc.2022.103608.

[35] A. López, M. Fernández, H. Rodríguez, F. Ferrero, O. Postolache, Development of an EOG-based system to control a serious game, Measurement 127 (June) (2018) 481–488, http://dx.doi.org/10.1016/j.measurement.2018.06.017.

[36] X. Zheng, X. Li, J. Liu, W. Chen, Y. Hao, A portable wireless eye movement-controlled human-computer interface for the disabled, Signal Process. (2009) 1–5.

[37] R. Barea, L. Boquete, J.M. Rodriguez-Ascariz, S. Ortega, E. López, Sensory system for implementing a human-computer interface based on electrooculography, Sensors 11 (1) (2011) 310–328, http://dx.doi.org/10.3390/s110100310.